The physics of pencil drawing

Aubin Archambault,[1] Lucie Domino,[1] and Vincent Bertin[1,2,*]

[1] *Aix Marseille Univ, CNRS, IUSTI UMR 7343, Marseille 13453, France*

[2] *Université Côte d'Azur, CNRS, INPHYNI UMR 7010, Nice 06200, France*

(Dated: July 22, 2026)

Abstract

Graphite-pencil drawing is a ubiquitous human activity, yet the physical mechanisms that control how material is transferred and produces shades remain poorly understood. At the microscale, sliding contact between a graphite lead and a rough substrate leads to the detachment and deposition of graphite fragments, a process analogous to mechanical wear in engineering systems. Such wear is typically described empirically by Archard's law, which relates macroscopic material loss to load and sliding distance but does not account for the microscopic processes governing debris formation. Here we show that pencil drawing provides a quantitative and versatile model system for wear, enabling a direct connection between microscopic fragmentation and macroscopic material transfer. Controlled experiments reveal that graphite exhibits unusually large wear coefficients under moderate loads, while producing debris with a scale-free, power-law size distribution spanning several decades in length scale. We demonstrate that this distribution is governed by the roughness of the substrate and is consistent with fragmentation processes on self-affine surfaces. Crucially, we establish a direct relationship between the debris size distribution and the optical intensity of the resulting graphite trace, linking the apparent grey level of a drawing to the surface coverage by fragments. This provides a physical framework for connecting microscopic fracture processes to macroscopic wear and visual appearance. More broadly, our work establishes pencil drawing as a simple and accessible experimental paradigm for investigating rough-contact wear, with implications ranging from tribology to the quantitative analysis of graphite and charcoal artworks.

* vincent.bertin@univ-cotedazur.fr

Pencil drawing produces patterns with continuously varying grey shades through the transfer of graphite onto a substrate during sliding contact. Artists exploit this transfer intuitively, tuning the shade through parameters such as normal force, drawing speed, pencil grade, lead sharpness, and paper texture. Yet the physical mechanisms governing graphite transfer and, ultimately, the shading remain unclear. At the microscale, graphite is not deposited as a uniform coating, but as discrete fragments that decorate the fibre network of the paper, accumulating along ridges and valleys where contact with the lead occurs (Fig. 1(a)). This morphology reveals pencil drawing as a rough-contact wear process, in which fragments are detached from the graphite lead and subsequently deposited onto the substrate (Fig. 1(d)).

More broadly, predicting material removal and transfer at sliding rough contacts remains a central challenge in wear physics and tribology [1, 2]. Macroscopic wear is commonly described by Archard's law [3, 4], $V/L = KF_N/\sigma_p$, where V is the transferred volume, L the sliding length, F_N the normal load, σ_p the material hardness and K a dimensionless wear coefficient. Although this empirical relation captures how wear scales with load, distance and hardness, the microscopic processes of contact, fracture and debris formation remain hidden inside the coefficient K [5–7]. Here, we show that pencil drawing exposes these processes directly, providing a simple model system that connects rough contact, graphite fragmentation and macroscopic material transfer. We further show how the resulting debris field determines the optical shade of the trace. By making both material loss and deposited fragments directly observable, this approach provides a new experimental route for investigating rough-contact wear and for quantitatively relating drawing materials, substrates and artistic techniques to visual appearance.

Pencil drawing set-up for wear investigations — To turn pencil drawing into a reproducible wear experiment, we built an automated drawing set-up that controls sliding distance, normal load, and drawing speed, while leaving the pencil free to move vertically (Fig. 1(b), Supp. Video 1 and Methods). We used graphite pencils spanning commercial grades from 4H to 6B, where H denotes hard pencils and B denotes bold, softer pencils. Because these grades are not defined by a standardized mechanical test and remain manufacturer dependent, we independently characterised the leads by microindentation. Their hardness varies by more than two orders of magnitude, from approximately 50 to 1,100 MPa

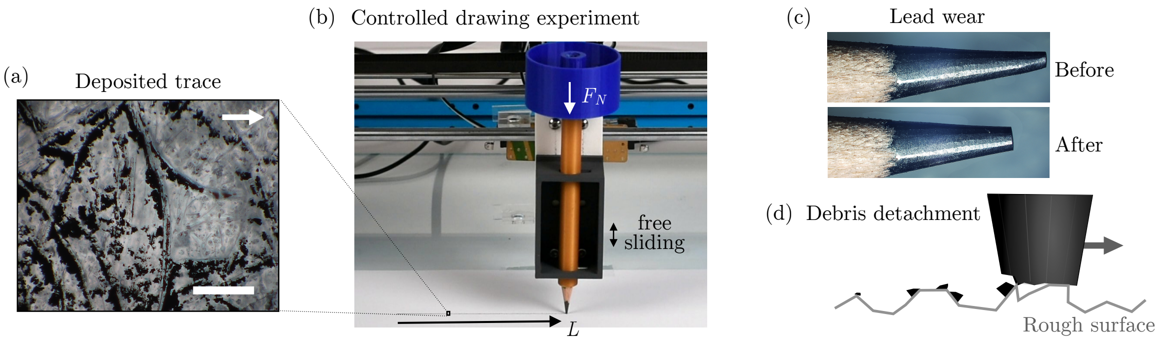

FIG. 1. **Pencil drawing as a model wear process.** (a) Optical micrograph of a graphite trace deposited on paper, revealing heterogeneous deposition of graphite fragments along the fibrous substrate texture. Arrow, sliding direction. Scale bar, 0.1 mm. (b) Controlled drawing experiment, with a graphite pencil mounted on an automated XY plotter. The normal load F_N is imposed using calibrated weights, while the custom holder constrains the pencil laterally and allows free vertical sliding. The image is extracted from Supplementary Video 1. The sliding length is denoted by L. (c) Optical images of the graphite lead before and after sliding, showing wear of the tip. (d) Schematic of debris generation at a rough contact: substrate asperities detach graphite fragments from the lead, which are subsequently deposited on the surface.

between 6B and 4H, reflecting the increasing clay content used to produce harder graphite–clay leads (Methods and Extended Data Table. 1) [8].

Most experiments were performed on standard printer paper, a representative fibrous rough substrate for drawing. We complemented these measurements with frosted glass substrates of controlled roughness, with h_{rms} ranging from 0.5 to 7 μm (Methods and Extended Data Fig. 2). This strategy allowed us to independently tune the two main material parameters controlling wear: lead hardness and counter-surface roughness.

Macroscopic wear — To quantify macroscopic wear, we imaged the pencil lead before and after sliding over a prescribed distance and measured the transferred volume (Fig. 1(c)). We first established the wear laws on frosted glass, whose controlled roughness provides cleaner and more reproducible measurements than paper, while retaining the same phenomenology observed on fibrous substrates. At fixed pencil grade and substrate roughness, the transferred volume increases linearly with both normal load (Fig. 2(a)) and sliding distance (Fig. 2(b)), consistent with Archard's law. This macroscopic wear rate is only weakly

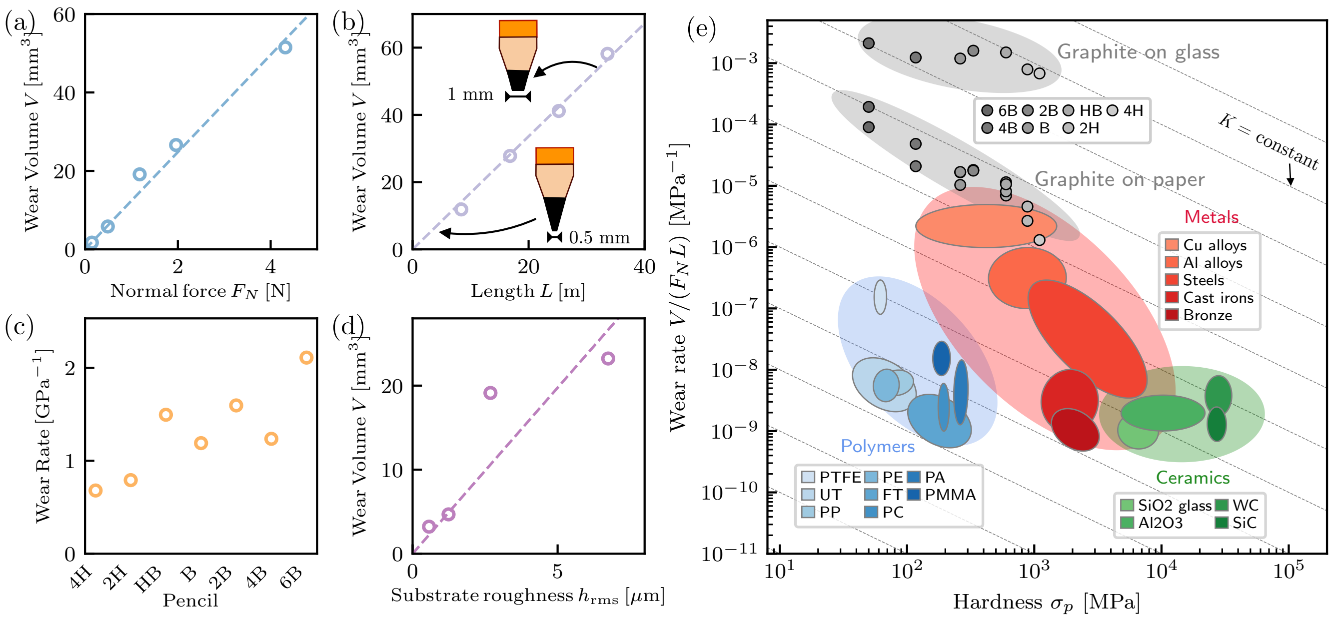

FIG. 2. **Macroscopic wear measurements.** (a) Wear volume as a function of normal load F_N, at fixed sliding length $L = 8.4\,\mathrm{m}$. The dashed line is a linear fit. (b) Wear volume transferred from the graphite lead as a function of sliding length L, at fixed normal load. The dashed line is a linear fit, consistent with Archard-like scaling. Insets show that changing the initial contact diameter of the lead, from approximately 0.5 mm for a freshly sharpened tip to 1 mm for a used tip, does not significantly affect the measured wear rate. (c) Normalized wear rate, $V/(F_N L)$, for graphite pencils of different grades, showing the strong influence of lead hardness. (d) Wear volume of an HB pencil on frosted glass substrates of different roughness. The wear volume increases with surface roughness, quantified here by the root-mean-square height. (e) Ashby-style map of wear rate $V/(F_N L)$ versus hardness σ_p. Coloured regions show typical ranges for polymers, metals and ceramics, extracted from Ref. [9]. Open circles show graphite-pencil wear measured on frosted glass and on paper. Graphite occupies a distinct region of the map, combining low hardness with efficient material transfer. Panels (a–d) use frosted glass to provide controlled roughness; panel (e) compares glass and paper.

affected by the initial contact geometry: freshly sharpened tips, with contact diameters of order 0.5 mm, and used tips, with diameters of order 1 mm, give comparable transferred volumes under otherwise identical conditions. Although the visual appearance of the trace may vary strongly, the total transferred volume is therefore primarily controlled by load, sliding distance, lead hardness, and substrate roughness. Normalizing the wear volume by normal force and sliding distance reveals a strong dependence on pencil grade (Fig. 2(c)), highlighting the central role of lead hardness.

We next asked how graphite-pencil wear compares with more conventional engineering materials. To this end, we placed our measurements on an Ashby-style map of wear rate, $V/(F_N L)$, versus hardness for a broad range of materials (Fig. 2(e)) [9, 10]. Using Archard's law, $V/(F_N L) = K/\sigma_p$, lines of constant K appear as straight lines of slope -1. Graphite occupies a distinct region of this space: it is comparatively soft, yet transfers efficiently, with $K \simeq 10^{-1} - 10^{0}$ on frosted glass and $K \simeq 10^{-3} - 10^{-2}$ on paper. This combination makes graphite well suited for writing, because substantial amounts of material can be deposited without requiring large contact forces, while pencil grading provides a broad tunability of wear rate. These same features have recently motivated the use of graphite pencils as model objects for studying shape evolution under stochastic mechanical wear [11].

The counter-surface is therefore a second key ingredient of drawing. For comparable root-mean-square roughness $h_{\rm rms}$, frosted glass produces wear rates approximately twenty to one hundred times larger than those measured on paper, showing that $h_{\rm rms}$ alone does not fully characterize the abrasive action of a surface. Controlled glass substrates further reveal the strong role of the roughness landscape: smooth float glass produces essentially no visible trace, whereas the wear rate increases systematically with the roughness of frosted glass (Fig. 2(d)). Thus, writing requires not only a soft, easily worn lead, but also a counter-surface rough enough to remove and retain graphite.

Microscopic debris distribution — Our macroscopic measurements establish pencil drawing as an Archard-like wear process. We now turn to the microscopic structure of the graphite trace to identify the processes hidden within this macroscopic law. Optical microscopy shows that graphite is not deposited as a continuous coating, but as a heterogeneous assembly of discrete wear debris spanning a broad range of sizes (Fig. 3(a)). The debris-area distribution follows a scale-free form over nearly four decades, with a probability density close to $P(\mathcal{A}) \sim \mathcal{A}^{-3/2}$. Similar power-law debris-size distributions have been reported in dry sliding wear of stainless steel, where they were linked to surface topography and microscopic contact events [12, 13]. This exponent is robust across pencil grades and normal loads. By contrast, changing the pencil hardness or the load shifts the upper cut-off

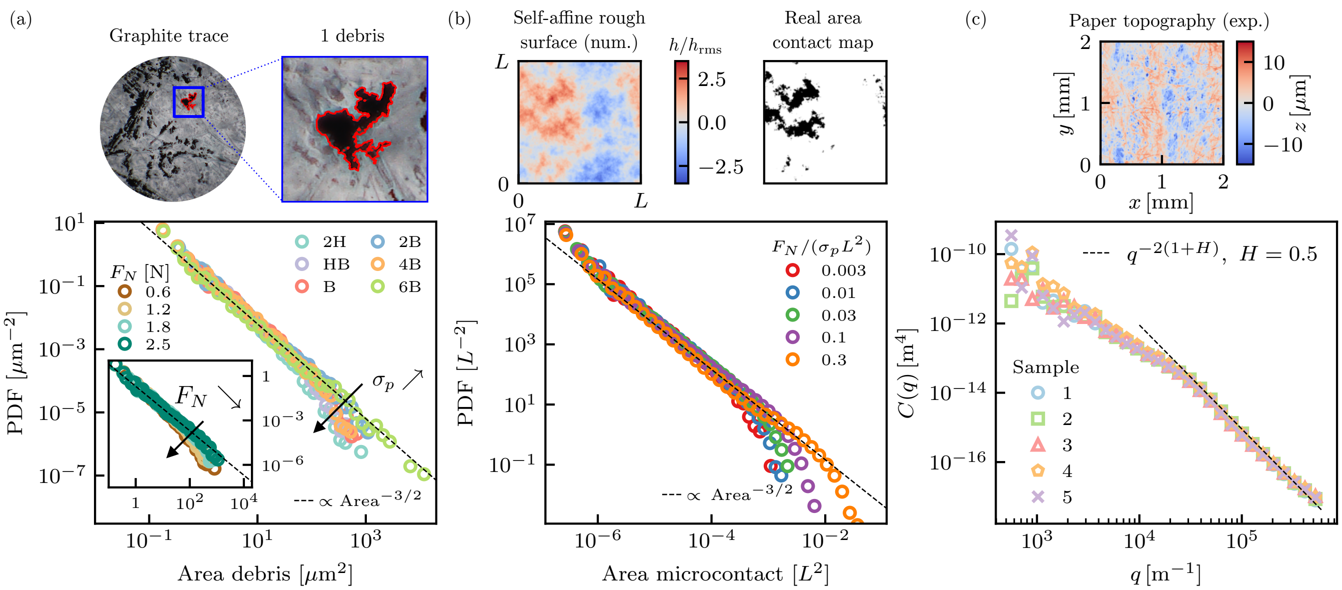

FIG. 3. **Scale-free debris statistics arise from self-affine rough contact.** (a) Graphite traces consist of discrete debris fragments whose area distribution follows $P(\mathcal{A}) \sim \mathcal{A}^{-3/2}$ over several decades. This scaling is robust to changes in pencil grade and normal load, while the upper cut-off varies with hardness and load. (b) Minimal rough-contact model. Numerically generated self-affine surfaces are brought into fully plastic contact, yielding disconnected real-contact maps. The contact map has $F_N/(\sigma_p L^2) = 0.1$. The resulting microcontact-area distributions reproduce the power-law regime and cut-off dependence observed for graphite debris. (c) Roughness characterization of the paper substrate. Profilometry reveals a self-affine topography, with a radially averaged height power spectral density $C(q) \sim q^{-2(1+H)}$ and $H \simeq 0.5$. The measured roughness statistics are used to generate the model surfaces in (b).

$\mathcal{A}_{\max}$, which sets the scale of the largest fragments. This cut-off is central. Because the decay exponent 3/2 is smaller than 2, the mean debris area is controlled by the largest events: $\langle \mathcal{A} \rangle \sim \int^{\mathcal{A}_{\max}} \mathcal{A} P(\mathcal{A})\, d\mathcal{A} \propto \mathcal{A}_{\max}^{1/2}$. Thus, although small fragments are the most numerous, the deposited graphite area is dominated by the rare largest fragments, whose size is set by $\mathcal{A}_{\max}$.

We next ask where this scale-free fragmentation law comes from, and what sets its upper cut-off. A natural starting point is the microscopic interpretation of Archard's law. For a rough contact in the fully plastic limit, the real area of contact $A_{\rm real}$ is much smaller than the nominal area and scales as $A_{\rm real} \sim F_N/\sigma_p$, as in the classical Bowden–Tabor picture of friction and more recent direct measurements of real contact area [14, 15]. This total real area is not continuous, but distributed over many disconnected microcontacts whose sizes are controlled by the roughness landscape. Within Archard's wear picture, these microcontacts are the elementary sites where wear debris can be generated: A_{real} sets the number and size of load-bearing junctions, while the wear coefficient K phenomenologically accounts for how often these junctions release detached fragments [4]. This interpretation suggests that the statistics of graphite debris may reflect the statistics of the underlying microcontacts.

To test this idea, we first characterised the substrate topography by profilometry. Paper consists of a disordered network of cellulose fibres, with typical diameters of order $5-15\,\mu$m, producing a rough landscape with no single characteristic lateral scale. Consistently, the measured topography exhibits self-affine roughness over the experimentally relevant range, with a height power spectral density $C(q) \sim q^{-2(1+H)}$ and $H \simeq 0.5$ (Fig. 3(c)). Self-affine descriptions are widely used in rough-contact mechanics, where they naturally lead to disconnected contact patches spanning a broad range of sizes [16–19]. More generally, threshold cuts through self-affine surfaces are known to generate scale-free island-area distributions, with exponents that depend on both the roughness exponent and the cut level [20]. We therefore generated numerical self-affine surfaces with the measured roughness statistics and computed the corresponding microcontact maps using a minimal fully plastic bearing-area model (Methods). Repeating this procedure over hundreds of digital surfaces of size $L \times L$ gives the distribution of microcontact areas for different values of the dimensionless load $F_N/(\sigma_p L^2)$. These simulated distributions reproduce the main features of the experimental debris statistics: a broad power-law regime, a comparable exponent, and an upper cut-off that increases with load or decreasing hardness (Fig. 3(b)). This agreement indicates that, to leading order, the geometry of rough contact sets the statistics of graphite fragmentation.

Shading — Having identified how graphite debris are generated, we now ask how this microscopic deposit becomes a macroscopic shade. At the scale of a drawing, individual debris are too small to be resolved by the eye, suggesting that visual intensity is governed not by the shape of each fragment, but by the coarse-grained fraction of paper covered by graphite. We therefore tested whether the gray level of a pencil drawing can be predicted from this local surface coverage by comparing an 8-bit scan of the drawing (Fig. 4(a)) with optical micrographs acquired across the same region. Approximately 1,000 micrographs

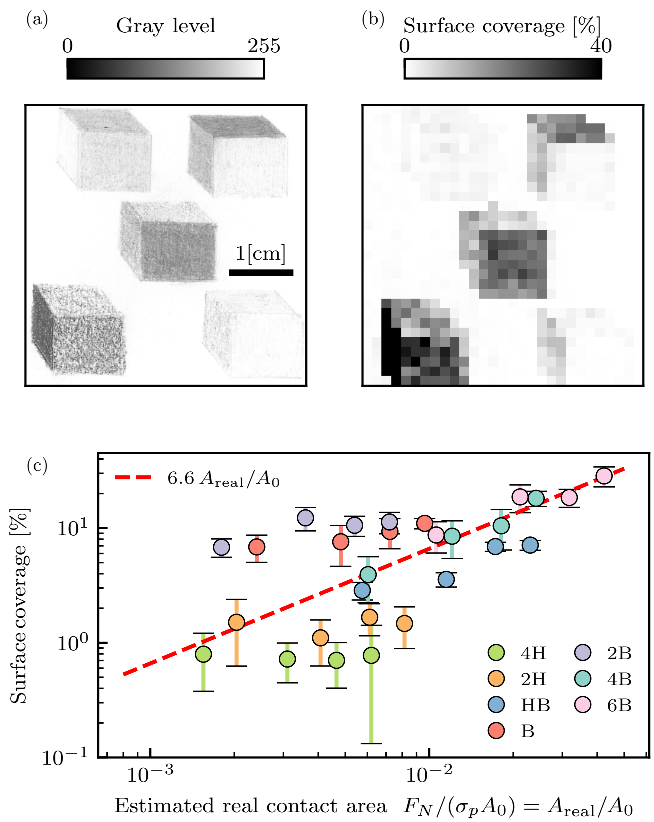

FIG. 4. **Pencil shade is controlled by graphite surface coverage.** (a) Scanned graphite drawing shown as an 8-bit grey-level map. Scale bar, 1 cm. (b) Surface-coverage map reconstructed from optical micrographs acquired across the same drawing, after segmentation of graphite-covered pixels and coarse-graining over $0.15 \times 0.15\,\mathrm{cm}^2$ regions. The coverage map reproduces the main contrast variations of the scanned image, showing that visual shade is governed by the local fraction of paper covered by graphite. (c) Surface coverage as a function of the estimated real contact fraction, $A_{\mathrm{real}}/A_0 \simeq F_N/(\sigma_p A_0)$, for different pencil grades and normal loads. The dashed line is a linear guide, $6.6\,A_{\mathrm{real}}/A_0$, indicating that graphite coverage scales with real contact area.

were segmented to extract the local graphite-covered area and reconstruct a spatial map of surface coverage (Fig. 4(b)). This coverage map reproduces the main contrast variations of the scanned drawing, confirming graphite surface coverage as the primary control parameter for pencil shading.

We next relate this optical quantity to the contact mechanics of drawing. Since the debris statistics originate from the population of microcontacts, we compare the measured surface coverage to the estimated fraction of real contact area, $A_{\mathrm{real}}/A_0 \simeq F_N/(\sigma_p A_0)$, where A_0 is the nominal lead–paper contact area estimated from the lead diameter. The two quantities increase together over the full set of pencil grades and loads, showing an approximate proportionality despite the simplicity of the fully plastic contact estimate (Fig. 4(c)). The dashed line corresponds to an empirical linear relation with prefactor of 6.6, indicating that the graphite-covered area exceeds the instantaneous real contact area. The fact that this prefactor exceeds unity is consistent with debris generated at microcontacts subsequently spreading, fragmenting, and accumulating within the surface texture, rather than remaining confined to the load-bearing junctions.

This simple picture does not fully describe the hardest pencil grades. Hard pencils, particularly 4H and 2H, deviate systematically from this simple scaling and show a weaker dependence on load. These deviations may partly reflect the limited optical resolution of the smallest graphite debris, although additional mechanisms cannot be excluded. Nevertheless, to zeroth order, the graphite surface coverage scales with the estimated real contact area. The remaining deviations point to additional mechanisms that remain to be clarified.

Discussion – We have shown that pencil drawing, an everyday activity, can be turned into a quantitative experiment on wear. A pencil trace is not simply a mark left on a surface, but the visible record of a rough-contact wear process. At the macroscopic scale, graphite displays unusually large wear coefficients, making it possible to deposit visible amounts of material under moderate loads, while the broad range of lead hardness provides a natural control parameter for wear rate and shading. At the microscopic scale, the deposited trace is composed of discrete graphite fragments with a broad, scale-free size distribution, whose scaling reflects the fractal nature of the rough surface and whose upper cut-off is controlled by load and hardness. At the optical scale, the apparent grey level is governed by the surface coverage of these fragments, which scales approximately with the estimated real area of contact.

Beyond pencil drawing itself, we anticipate that the experimental platform introduced here will provide a new route to address one of the central challenges of wear physics: deriving macroscopic wear laws from microscopic contact and fracture mechanisms. Recent theories have approached this problem from complementary perspectives, including critical-junction and energy-based particle detachment criterion [5–7, 21, 22], multiasperity interactions [23], and multiscale crack-growth models [10, 24–26]. The present platform provides a direct way to test these theoretical ideas by varying the substrate roughness, lead hardness, normal load and sliding history, while directly imaging the resulting debris field. Here, we focused on drawing on initially clean surfaces. A natural next step is repeated sliding, where deposited graphite becomes a third body: it can carry load, lubricate the contact, and limit subsequent wear [27–30]. More broadly, extending this approach to other drawing materials, such as charcoal and pastels, could provide quantitative tools for conservation science by relating material choice, substrate texture and artistic technique to the resulting deposit and visual appearance [31, 32].

DATA AVAILABILITY

The data supporting the findings of this study are available from the corresponding author upon reasonable request.

CODE AVAILABILITY

The code used for image analysis, numerical surface generation and microcontact analysis is available from the corresponding author upon reasonable request.

ACKNOWLEDGEMENTS

We thank Olivier Pouliquen for his continuous support and many insightful discussions, Lucas Frérot for insightful discussions on wear modelling, Kilian Laclavetine, Emeline Pouyet and Leila Sauvage for discussions on conservation science, Laurence Bergougnoux for help with Arduino interfacing, Joël Marthelot for providing the XY plotter, Yoël Forterre for help with microindentation measurements, and Nathalie Ehret for profilometry measurements.

FUNDING

This project has received funding from the European Research Council (ERC) under the European Union's Horizon programme (Grant No. 101097842), which supported A.A. and V.B. Views and opinions expressed are, however, those of the author(s) only and do not necessarily reflect those of the European Union or the European Research Council. Neither the European Union nor the granting authority can be held responsible for them. L.D. acknowledges support from Institut Mécanique et Ingénierie (IMI).

AUTHOR CONTRIBUTIONS

A.A., L.D. and V.B. designed the project, performed the experiments, and analysed the data. V.B. wrote the manuscript with input from all authors.

COMPETING INTERESTS

The authors declare no competing interests.

ADDITIONAL INFORMATION

Correspondence and requests for materials should be addressed to V.B.

Methods

Drawing experiments. Controlled drawing experiments were performed using a modified Makeblock XY plotter operated as a computer-controlled writing stage. The in-plane motion was prescribed by custom Arduino/CNC commands, which set the drawing speed to 2 cm/s, as well as the trajectory and total sliding distance. The original pen holder was replaced by a custom 3D-printed pencil holder designed to constrain the pencil laterally while allowing it to slide freely in the vertical direction. The normal load was imposed by adding calibrated weights directly above the pencil and was independently measured. Loads in the range 50-250 g were used for paper substrates; larger loads were avoided because they produced irreversible deformation of the paper. For frosted-glass substrates, loads between 20 and 400 g were used.

Experiments were performed either on standard printer paper (Inacopia, 70 g/m^2) or on frosted-glass substrates of controlled roughness. Paper sheets were taped onto a smooth Plexiglas plate to provide a flat and reproducible backing. The glass substrates were commercial N-BK7 ground-glass diffusers with different grit values (Thorlabs), allowing the counter-surface roughness to be varied systematically. For each experiment, the pencil was translated along straight lines over a prescribed total sliding distance, typically between 4 and 100 m. Successive lines were spatially separated so that the pencil did not pass repeatedly over the same trace, ensuring that each stroke corresponded to contact with a fresh region of the substrate.

Mechanical characterization of pencil leads. The mechanical properties of the graphite leads were measured with a Hysitron TI Premier nanoindenter equipped with a Berkovich TI 0039 diamond tip. We characterised commercial BIC graphite pencils spanning grades from 6B to 4H. For each pencil, the wood casing was first removed with a razor blade. The exposed lead was then cut into short segments and bonded to a glass slide using epoxy glue, in order to provide a stable sample during indentation. After curing, the samples were placed in the microindenter, and 16 independent indentations were performed for each pencil grade. The indentation curves were analysed to extract the hardness σ_p and reduced elastic modulus $E^* = E/(1-\nu^2)$, with E the Young's modulus and ν the Poisson's ratio. The full set of measured values is reported in Table I

Characterization of the surfaces. Surface topographies were measured with a chromatic

TABLE I. Mechanical properties of graphite pencil leads measured by instrumented microindentation.

Pencil grade	Hardness σ_p (MPa)	Reduced modulus E^* (GPa)
6B	50	3.50
4B	117	3.90
2B	332	9.35
B	262	8.34
HB	600	13.0
2H	884	19.6
4H	1,100	18.1

confocal optical pen (CCS-Prima, 150 μm probe) operated in surface-scanning mode. Each surface was scanned on a regular square grid with a lateral step of 1.3 μm, yielding height maps over 2×2 mm^2 fields of view. Invalid or missing points were replaced by nearest-neighbour interpolation before further analysis. To remove the residual tilt of the sample, each height map $h(x, y)$ was fitted by a plane $ax+by+c$, which was then subtracted from the raw topography. The root-mean-square roughness h_{rms} was computed from the corrected height fluctuations. A typical topography of our printer paper is shown in Fig. 3(c).

The roughness spectrum was obtained from the two-dimensional Fourier transform of the flattened topography. We then computed the power spectral density $C(q_x, q_y) \propto |\hat{h}(q_x, q_y)|^2$, where q_x and q_y are the spatial frequencies in the two in-plane directions. The isotropic spectrum $C(q)$ was then obtained by radial averaging in logarithmic bins, with $q = (q_x^2 + q_y^2)^{1/2}$. The Hurst exponent was extracted by fitting the self-affine scaling regime, $C(q) \sim q^{-2(1+H)}$. Spectra for 5 different paper sheets are shown in Fig. 3(c).

The topographies and spectra of the frosted glass surfaces are shown in Fig. 5. The surfaces were sandblasted using abrasive grains of different sizes, with grain size increasing as the grit number decreases. As expected, both the roughness amplitude and the lateral correlation length increase with decreasing grit number. The measured roughness values h_{rms} are reported in Table II and are consistent with those reported in Ref. [33] for surfaces from the same supplier.

The raw topography data are available on the platform contact.engineering [34].

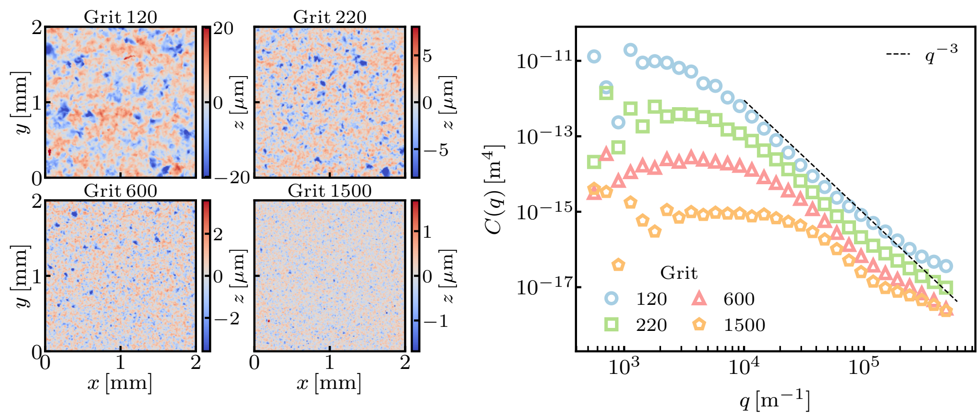

FIG. 5. **Roughness characterization of frosted glass substrates.** Topography maps of frosted glass substrates with grit sizes 120, 220, 600 and 1500. Each map shows a $2 \times 2\,\mathrm{mm}^2$ region after detrending, with an individual colour scale set by the corresponding roughness amplitude. The roughness decreases systematically with increasing grit number. Right, radially averaged height power spectral density $C(q)$ of the same surfaces. The spectra show a broad self-affine regime compatible with $C(q) \sim q^{-3}$, corresponding to a Hurst exponent $H \simeq 0.5$. These substrates provide controlled rough counter-surfaces for the graphite wear experiments.

TABLE II. Roughness of frosted glass surfaces measured with chromatic confocal optical pen.

Grit	Roughness h_{rms} (μm)
120	6.74
220	2.68
600	1.24
1500	0.57

Debris-size analysis. The size distribution of graphite debris was measured from optical micrographs of pencil traces acquired with a HIROX RH-2000 microscope equipped with a MXB-2500REZ / 5000REZ objective. Images were recorded as 1920×1200-pixel RGB micrographs with a resolution of $0.40\,\mu$m per pixel. For each pencil grade, 4 to 10 independent micrographs were analysed. To avoid edge artefacts and illumination variations near the border of the field of view, the analysis was restricted to a fixed circular region of interest. Images were converted to grayscale, and graphite debris were segmented by applying a fixed intensity threshold, with pixels below the threshold identified as graphite.

Connected graphite pixels were then labelled as individual debris, and the area of each connected component was measured. Pixel areas were converted into physical areas using the optical calibration. The debris areas obtained from the different micrographs were pooled for each pencil grade and converted into probability density functions using logarithmically spaced area bins.

Randomly rough surface generation. Numerical self-affine surfaces were generated in Fourier space. We considered a square periodic domain of size $L \times L$, discretized on an $N \times N$ grid. Without loss of generality, we set $L = 1$ and used $N = 2048$. For each Fourier mode of spatial frequency $q = (q_x^2 + q_y^2)^{1/2}$, we prescribed an isotropic height power spectral density $C(q) \propto q^{-2(1+H)}$, where H is the Hurst exponent. This power law was imposed only over a finite range of wavelengths, $\lambda_{\mathrm{min}} = 0.001 < \lambda < \lambda_{\mathrm{max}} = 0.1$, corresponding to $q_{\mathrm{min}} = 1/\lambda_{\mathrm{max}}$ and $q_{\mathrm{max}} = 1/\lambda_{\mathrm{min}}$. Modes with $q < q_{\mathrm{min}}$ were assigned a constant spectral amplitude, while modes with $q > q_{\mathrm{max}}$ were suppressed. Each Fourier mode was then assigned a random phase uniformly distributed between 0 and 2π [35]. The surface height field was obtained by inverse Fourier transform, after which the mean height was subtracted and the field was rescaled to have a unit rms roughness. Different random seeds were used to generate independent realizations with identical statistical properties.

Microcontact maps (Fig. 3(b)) were computed from the generated self-affine surfaces using a minimal fully plastic bearing-area model. For a prescribed dimensionless load, written as a target real contact fraction $A_{\mathrm{real}}/L^2 = F_N/(\sigma_p L^2)$, we selected the highest points of the height field until this prescribed area fraction was reached. This operation defines a binary contact map, in which contacting pixels are those for which $h(x, y)$ exceeds the associated height threshold. Connected contacting pixels were then identified using an eight-neighbour connectivity criterion, and the area of each connected component was measured as a microcontact area. The procedure was repeated over 100 statistically independent surface realizations and for several prescribed contact fractions, $A_{\mathrm{real}}/L^2 = 0.003$, 0.01, 0.03, 0.1, and 0.3. The resulting microcontact areas were pooled for each load and converted into probability density functions using logarithmic area bins.

Supplementary Video 1 — Controlled pencil-drawing experiment. The video shows the automated drawing apparatus used to perform reproducible pencil-wear experiments. A

6B graphite pencil is mounted in a custom holder attached to an XY plotter, which controls the trajectory and sliding distance. The pencil is free to slide vertically inside the holder, so that the applied weight (here, 140 g) sets the normal load while the tip remains in contact with the substrate during drawing.

[1] L. Pastewka, A. I. Vakis, S. J. Eder, R. Aghababaei, A. Almqvist, G. Carbone, M. Chandross, D. Dini, H. J. Ehrich, J. P. Ewen, *et al.*, Modeling in tribology: Recent advances, applications, and open questions, Tribology International **218**, 111326 (2026).

[2] R. Xu, W. Sheng, F. Zhou, and B. Persson, Rubber wear: History, mechanisms, and perspectives, Tribology Letters **73**, 90 (2025).

[3] J. Burwell and C. Strang, On the empirical law of adhesive wear, Journal of Applied Physics **23**, 18 (1952).

[4] J. Archard, Contact and rubbing of flat surfaces, Journal of Applied Physics **24**, 981 (1953).

[5] E. Rabinowicz, The effect of size on the looseness of wear fragments, Wear **2**, 4 (1958).

[6] R. Aghababaei, D. H. Warner, and J.-F. Molinari, Critical length scale controls adhesive wear mechanisms, Nature Communications **7**, 11816 (2016).

[7] L. Frérot, R. Aghababaei, and J.-F. Molinari, A mechanistic understanding of the wear coefficient: From single to multiple asperities contact, Journal of the Mechanics and Physics of Solids **114**, 172 (2018).

[8] Y. Kim, A. Sung, Y. Seo, S. Hwang, and H. Kim, Measurement of hardness and friction properties of pencil leads for quantification of pencil hardness test, Advances in Applied Ceramics **115**, 443 (2016).

[9] M. F. Ashby, "The CES EduPack resource booklet 2: Material and process selection charts," (2009).

[10] M. Ciavarella, Some remarks on a recent wear theory, Tribology Letters **73**, 55 (2025).

[11] J. Sebastian and K. H. Jensen, The geometry of Nature's stingers is universal due to stochastic mechanical wear, Proceedings of the National Academy of Sciences **123**, e2526098123 (2026).

[12] J. L. Xuan, H. S. Cheng, and R. J. Miller, Generation of Submicrometer Particles in Dry Sliding Contact, Journal of Tribology **112**, 684 (1990).

[13] J. Xuan and H. Cheng, *Tribology Series*, Paper VI (iii) Microscopic Wear Debris Generation

and Surface Topography **21**, 247 (1992).

[14] F. P. Bowden and D. Tabor, *The friction and lubrication of solids*, Vol. 9 (Oxford University Press, 2001).

[15] B. Weber, T. Suhina, T. Junge, L. Pastewka, A. Brouwer, and D. Bonn, Molecular probes reveal deviations from Amontons' law in multi-asperity frictional contacts, Nature Communications **9**, 888 (2018).

[16] A. Majumdar and B. Bhushan, Fractal Model of Elastic-Plastic Contact Between Rough Surfaces, Journal of Tribology **113**, 1 (1991).

[17] S. Hyun, L. Pei, J.-F. Molinari, and M. O. Robbins, Finite-element analysis of contact between elastic self-affine surfaces, Physical Review E—Statistical, Nonlinear, and Soft Matter Physics **70**, 026117 (2004).

[18] L. Pei, S. Hyun, J.-F. Molinari, and M. O. Robbins, Finite element modeling of elasto-plastic contact between rough surfaces, Journal of the Mechanics and Physics of Solids **53**, 2385 (2005).

[19] J. M. Monti, L. Pastewka, and M. O. Robbins, Fractal geometry of contacting patches in rough elastic contacts, Journal of the Mechanics and Physics of Solids **160**, 104797 (2022).

[20] Z. Olami and R. Zeitak, Scaling of island distributions, percolation, and criticality in contour cuts through wrinkled surfaces, Physical Review Letters **76**, 247 (1996).

[21] R. Aghababaei, D. H. Warner, and J.-F. Molinari, On the debris-level origins of adhesive wear, Proceedings of the National Academy of Sciences **114**, 7935 (2017).

[22] J. Choudhry, A. Almqvist, and R. Larsson, Improving Archard's wear model: an energy-based approach, Tribology Letters **72**, 93 (2024).

[23] R. Aghababaei, T. Brink, and J.-F. Molinari, Asperity-level origins of transition from mild to severe wear, Physical Review Letters **120**, 186105 (2018).

[24] B. Persson, R. Xu, and N. Miyashita, Rubber wear: Experiment and theory, The Journal of Chemical Physics **162**, 074704 (2025).

[25] R. Xu and B. Persson, Sliding wear: role of plasticity, Tribology Letters **73**, 109 (2025).

[26] M. Ciavarella, Wear due to fatigue initiation, Tribology International **207**, 110592 (2025).

[27] M. Godet, The third-body approach: a mechanical view of wear, Wear **100**, 437 (1984).

[28] I. L. Singer, How third-body processes affect friction and wear, MRS Bulletin **23**, 37 (1998).

[29] F.-C. Hsia, F. M. Elam, D. Bonn, B. Weber, and S. E. Franklin, Wear particle dynamics drive

the difference between repeated and non-repeated reciprocated sliding, Tribology International **142**, 105983 (2020).

[30] P. Alavi, L. Rocchi, C. Leppin, J. Molinari, and G. Anciaux, A multiscale model of friction considering the influence of third-body wear particles, Wear **596**, 206719 (2026).

[31] N. S. Daly, M. Sullivan, L. Lee, J. K. Delaney, and K. Trentelman, Odilon Redon's noir drawings: characterization of materials and methods using noninvasive imaging and spectroscopies, Heritage Science **7**, 1 (2019).

[32] L. Brunel-Duverger, L. de Viguerie, V. Georges, J. Le Bellego, L. Sauvage, and E. Pouyet, Toward spectral continuum: Multimodal non-invasive analysis of historical pastels, Journal of Cultural Heritage **64**, 49 (2023).

[33] M. A. Quetzeri-Santiago, A. A. Castrejón-Pita, and J. R. Castrejón-Pita, The effect of surface roughness on the contact line and splashing dynamics of impacting droplets, Scientific Reports **9**, 15030 (2019).

[34] M. C. Röttger, A. Sanner, L. A. Thimons, T. Junge, A. Gujrati, J. M. Monti, W. G. Nöhring, T. D. Jacobs, and L. Pastewka, Contact. engineering—Create, analyze and publish digital surface twins from topography measurements across many scales, Surface Topography: Metrology and Properties **10**, 035032 (2022).

[35] J.-J. Wu, Simulation of rough surfaces with FFT, Tribology International **33**, 47 (2000).